# Local Pulmonary Structure Classification for Computer-Aided Nodule Detection

Claus Bahlmann[a], Xianlin Li[b] and Kazunori Okada[a]

[a]Siemens Corporate Research, Inc., 755 College Road East, Princeton, NJ 08540, USA
[b]Harvard University, 1842 Harvard Yard Mail Center, Cambridge, MA 02138, USA

## ABSTRACT

We propose a new method of classifying the local structure types, such as nodules, vessels, and junctions, in thoracic CT scans. This classification is important in the context of computer aided detection (CAD) of lung nodules. The proposed method can be used as a post-process component of any lung CAD system. In such a scenario, the classification results provide an effective means of removing false positives caused by vessels and junctions thus improving overall performance. As main advantage, the proposed solution transforms the complex problem of classifying various 3D topological structures into much simpler 2D data clustering problem, to which more generic and flexible solutions are available in literature, and which is better suited for visualization. Given a nodule candidate, first, our solution robustly fits an anisotropic Gaussian to the data. The resulting Gaussian center and spread parameters are used to affine-normalize the data domain so as to warp the fitted anisotropic ellipsoid into a fixed-size isotropic sphere. We propose an automatic method to extract a 3D spherical manifold, containing the appropriate bounding surface of the target structure. Scale selection is performed by a data driven entropy minimization approach. The manifold is analyzed for high intensity clusters, corresponding to protruding structures. Techniques involve EM clustering with automatic mode number estimation, directional statistics, and hierarchical clustering with a modified Bhattacharyya distance. The estimated number of high intensity clusters explicitly determines the type of pulmonary structures: nodule (0), attached nodule (1), vessel (2), junction (>3). We show accurate classification results for selected examples in thoracic CT scans. This local procedure is more flexible and efficient than current state of the art and will help to improve the accuracy of general lung CAD systems.

**Keywords:** Computer-Aided Diagnosis, CT, Pulmonary Nodules, Statistical Clustering, Directional Statistics

## 1. INTRODUCTION

Lung cancer is responsible for over 160,000 deaths in the past year in the United States alone. While not smoking is the best prevention against lung cancer, early detection is the key to improving patient prognosis. When the cancer is detected early and surgery is performed, the 5-year survival rate for patients with stage I non-small-cell lung cancer is 60% to 80%. However, patients who do not have surgery face a 5-year survival rate of only 10%.[1]

Imaging techniques such as computer tomography (CT) scans offer noninvasive and sensitive approaches to early detection. Computer-aided detection and diagnosis (CAD) of lung nodules in thoracic CT scans decreases the possibility of human error for a more efficient and standardized diagnostic process. In CT scans, lung nodules appear as dense masses of various shapes and sizes. They may be isolated from or attached to other structures such as blood vessels or the pleura.

Recently a number of techniques have been proposed for automated detection and classification of nodules in thin-slice CT including: region growing and automatic threshold determination,[2] template matching with Gaussian nodule models,[3] using 3D nodule selective and noise suppressing filters,[4] nodule matching,[5] and deformable geometrical and intensity templates.[6]

One of the main shortcomings of these state of the art CAD systems is the difficulty associated with differentiating between nodules and other dense structures such as blood vessels. Due to the circular-shape assumptions used in most of the systems, curved vessels and their junctions are often incorrectly detected as nodules, resulting in false positive (FP)

Further author information:
C. B.: E-mail: claus.bahlmann@siemens.com
X. L.: E-mail: li3@fas.harvard.edu
K. O.: E-mail: kazunori.okada@siemens.com

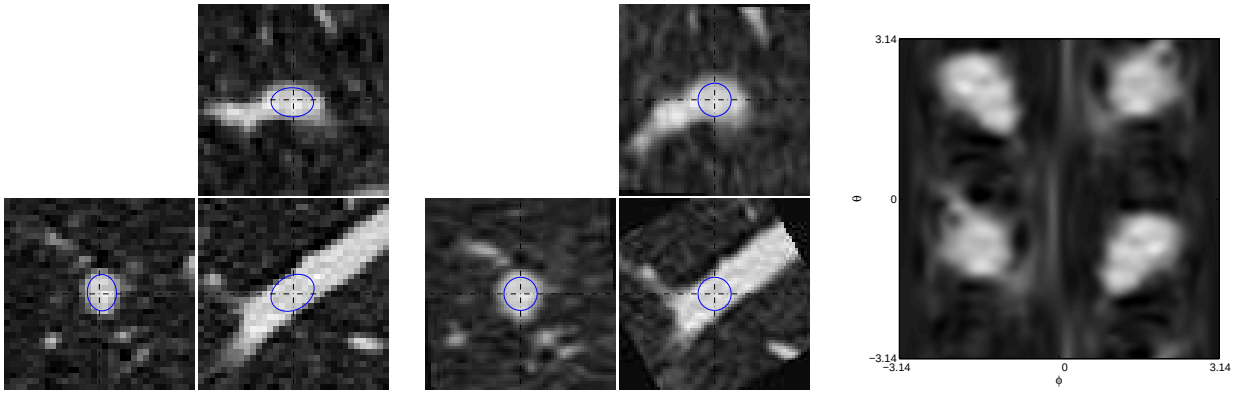


(a) VOI and segmented nodule candidate (b) Affine-normalized VOI (c) Unwrapped, spherical parameterization of the bounding manifold

**Figure 1.** Proposed method for pulmonary structure classification. Subfigure (a) shows the original voxel of interest (VOI), with ellipsoid fitted nodule structure, here a vessel. The ellipsoid fitting is obtained from our segmentation module. Subfigure (b) represents an affine-normalization of the original VOI, in that the ellipsoid is warped to an isotropic sphere. Subfigure (c) represents a bounding manifold of the segmented structure at distance $r_{\text{bound}}$, unwrapped to a 2D image and parameterized by the spherical polar coordinates $\theta$ and $\phi$. Image grayscale values have been obtained via tri-linear interpolation.

cases. To reduce the number of such FPs, two types of solutions have been proposed previously: correlation-based filters to enhance the area of interest with fuzzy shape analysis for vessel tree reconstruction[7] and a method utilizing tracking of the vessels medial axis given by Hessian-based analysis.[8] The drawbacks of the former approach include its inflexibility. Simple structural templates used in the study will not handle many complex vascular shapes and topologies. On the other hand, the latter approach is computationally very expensive while being able to handle more irregular structures.

In this paper, we propose a novel method of classifying local structure types, such as nodules, attached nodules, vessels, and junctions, in thoracic CT scans. This solution is envisioned to serve as a post-process filter within an overall lung CAD system so as to reduce FPs caused by the vessels and junctions. This study thus assumes that positive candidates are provided by such a CAD system or from radiologist's report, focusing on the problem of FP reduction.

The proposed method first fits an anisotropic Gaussian model to data by using a previously published one-click segmentation method.[9] Using the fitted anisotropic Gaussian spread, the data domain is affine-normalized so as to warp the anisotropic ellipsoid into a fixed-size isotropic sphere. Next a 3D spherical manifold, containing the bounding surface of the target structure, is automatically extracted. We propose an entropy-based data-driven solution for this manifold extraction. The extracted 3D manifold in Cartesian coordinates will form a 2D image in spherical coordinates. This 2D bounding manifold image contains some high intensity clusters whose number depends on the structure types. For a nodule, attached nodule, vessel, or junction, there must be 0, 1, 2 or >3 number of clusters, respectively. Thus we can apply a clustering analysis to the manifold image and classify the structure type according to the estimated cluster numbers. Importantly, this association of the cluster numbers and the structure types holds true regardless of vast geometrical and topological variability of target structures. This endows the presented method with favorable flexibility against the variabilities.

Moreover, the proposed approach in effect transforms the difficult topological classification problem into a generic 2D clustering problem which can be solved much easily by using many well-studied solutions. We propose an EM-based clustering solution by fitting a Gaussian mixture model to samples drawn from the bounding manifold image. It extends a recently proposed Gaussian fitting method, including automatic mode number selection,[10] with the use of directional statistics, in particular a multivariate wrapped Gaussian modeling.[11]

Beyond the scope of lung CAD, the presented classification method can be used to provide meaningful information of vascular structures in various domains such as angiography.

The rest of paper is organized as follows. In the following section, we give a complete overview of the proposed pulmonary structure recognition approach. Section 3 illustrates and verifies the feasibility by experiments with thoracic CT scan data. Section 4 concludes this contribution.

## 2. PROPOSED METHOD FOR PULMONARY STRUCTURE CLASSIFICATION

The proposed classification solution is envisioned to serve as a post-process filter within a lung CAD system so as to reduce FPs caused by the vessels and junctions. In this setting, it is assumed that approximate locations of pulmonary structures are present, for instance, from an above mentioned a CAD system, a radiologists manual reading, or reports.

### 2.1. Local pulmonary structure segmentation

A previously developed one-click nodule segmentation algorithm[9] is used to locate and segment target structures including nodules, attached nodules, vessels, and vessel junctions. Nodule candidate locations, provided *a priori*, serve as initialization to this semi-automatic segmentation solution.

This algorithm is based on robustly fitting an anisotropic Gaussian-based intensity model to the data using Gaussian scale-space mean shift analysis and Jensen-Shannon divergence-based automatic bandwidth selection. This segmentation solution provides a precise estimate of target center from imprecise CAD or manual initialization. The robustness of this solution also allow it to segment non-nodule areas such as vessels and vessel junctions/branches of our interest. An example of this segmentation result is shown in Figure 1 (a).

### 2.2. Structure classification

In the setting of a nodule detection application, incorrectly detected and segmented vessel and vessel branch structures represent a FP case. Main contribution of this paper is a classification method, which is targeted to reject all such non-nodule structures, and, as a byproduct, to infer the category of the type of pulmonary structure under consideration, that is, nodule, attached nodule, vessel, or vessel junction.

As will be explained, it is based on cluster analysis of an appropriate manifold, computed from the bounding area of the target structure. The number of high intensity clusters in this analysis will directly determine the pulmonary structure class.

#### 2.2.1. Bounding manifold construction

Structure classification in the original 3D image space is usually a theoretically involved and computationally complex problem. To overcome these difficulties, we propose to perform the classification in a less complex domain. Apart from the computational benefits, such an approach has the advantage of a more generic and flexible inventory of analysis techniques and more illustrative visualization potentiality, which is especially important in the context of a possible interaction with the radiologist.

In particular, we consider an ellipsoidal manifold in 3D to be extracted from the target structure boundary. Ellipsoid fitting is usually not a trivial problem, however, this task is alleviated by our choice of the local structure segmentation, which gives accurate estimates of center and ellipsoidal shape of the nodule in terms of the Gaussian parameters mean and covariance.

In the following, we will explain the construction of the bounding manifold. Illustrative aids with an exemplary case are provided in Figure 1.

**Affine-normalization** In order to simplify the mathematical representation, the original volume of interest (VOI), illustrated in Figure 1 (a), is affine-normalized. In other words, we warp the VOI such that the segmented anisotropic ellipsoid is transformed to a fixed-sized isotropic sphere, placed at the center of the VOI. Figure 1 (b) shows the affine-normalized VOI.

The parameters of the affine-normalization, that is, scaling directions and factors, can be straightforwardly obtained from an eigenvalue analysis of the structure covariance estimated by the segmentation module.

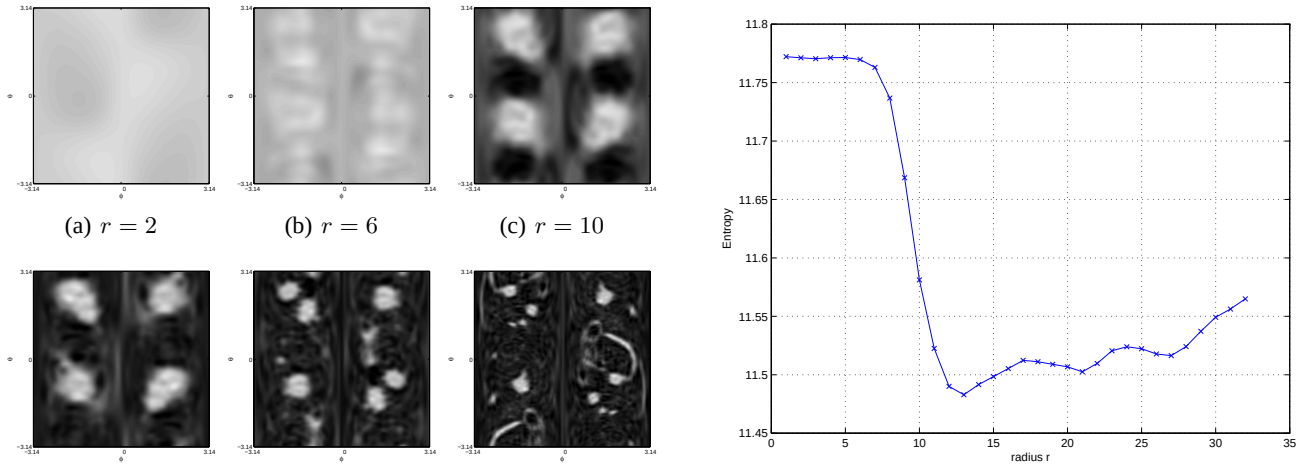


(a) $r = 2$ (b) $r = 6$ (c) $r = 10$

(d) $r = 13$ (e) $r = 18$ (f) $r = 28$ (g) Entropy

**Figure 2.** Unwrapped ellipsoids of different radii $r$ and the respective image intensity histogram entropy. These characteristics allow a data driven radius selection for the bounding manifold.

**Spherical manifold construction** A manifold is constructed from the affine-normalized 3D image. Geometrically, it is aimed to represent a spherical layer slightly beyond the target structure bounding surface, such that it contains information about protruding objects passing through the surface. Its shape is assumed ellipsoidal in the original VOI, in particular, proportional to the ellipsoid obtained from the anisotropic Gaussian-based segmentation. Hence, in the affine-normalized representation it corresponds to an isotropic spherical shape as well, defined by center point $(a_{\text{bound}}, b_{\text{bound}})$ and radius $r_{\text{bound}}$. Whereas the center point is identical with the one of the segmented ellipsoid, the spherical radius $r_{\text{bound}}$ will be determined in a data driven way, as will be explained shortly.

Assuming a fixed $r_{\text{bound}}$, the bounding manifold representation can be transformed from Cartesian $(x, y, z)$ to the spherical coordinates $(\theta, \phi)$. Here, $\theta$ refers to the azimuth, and $\phi$ to the polar angle. The result is an "unwrapped" representation of the affine-normalized ellipsoid as a 2D image matrix $I(\theta, \phi)$. Figure 1 (c) illustrates the result for our well-known example. Note that there, contrary to common convention, the polar angle ranges over an interval of $\text{Interval}_\phi = 2\pi$ (instead of $\pi$), that is, $\phi \in [-\pi, \pi]$, resulting in a double occurrence of the Cartesian voxels. The reason for introducing this redundancy is that the clustering, which will be introduced in Section 2.2.2, requires a periodic behavior of $I(\theta, \phi)$ in both parameters over their respective intervals $\text{Interval}_\theta$ and $\text{Interval}_\phi$, that is, $I(\theta + \text{Interval}_\theta, \phi + \text{Interval}_\phi) = I(\theta, \phi)$. For the case of spherical coordinates, this is obviously not fulfilled, if $\text{Interval}_\phi = \pi$.

We now explain the determination of the appropriate radius $r_{\text{bound}}$. We advice a data driven approach, based on the entropy of the intensity distributions. To motivate this approach, consider Figures 2 (a)–(f), each of which illustrates the unwrapped ellipsoid representation in the $(\theta, \phi)$-domain with different radii $r$. Figure 2 (g) shows the entropy $E_r$, computed on image intensities, for radii $r \in \{1, \ldots, 32\}$. We treat the unwrapped manifold image as a 2D likelihood function after normalizing the CT intensity value distribution appropriately. Then intensity entropy is computed directly with the normalized intensity values interpreted as probability values. The goal of radius selection is to automatically choose a radius such that high intensity clusters, due to protruding structures, appear most distinctively in the corresponding manifold. Such manifold image, consisting of a few clusters as shown in Figure 2 (d), should have lower entropy than images with smaller and larger radii due to the following intuitive arguments. The smaller radii makes the corresponding bounding ellipsoids go through inside target structures, resulting in high entropy values with more flat likelihoods as shown in Figures 2 (a)–(b). On the other hand, the larger radii also causes high entropy due to appearance of other "non-target" structures located nearby as shown in Figures 2 (e)–(f). Therefore the appropriate radius $r_{\text{bound}}$forms a local minimum of the entropy distribution $E_r$.

In this respect, we choose $r_{\text{bound}}$ to be located at the first appearance of a positive difference quotient $\frac{\Delta E_r}{\Delta r}$, that is,

$$r_{\text{bound}} = \min_r \{ r \,|E_{r+1} > E_r \} .$$

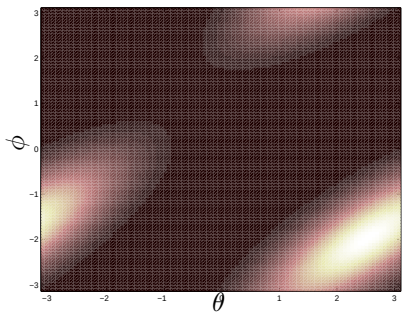


**Figure 3.** A problem of clustering with directional data. An appropriate clustering algorithm in the directional $(\theta, \phi)$-domain should recover a single cluster. However, with a linear instead of directional modeling, each of the three observable structures would form an independent cluster.

### 2.2.2. Cluster analysis of the bounding manifold

Having transformed parts of the 3D pulmonary structure to a 2D image, we can apply well-studied, efficient, and easily visualizable 2D image analysis techniques. As can be seen from Figure 1 (c), the bounding manifold contains valuable information for pulmonary structure classification. In fact, the *number of high intensity clusters* exposes the type of the pulmonary structure, being equivalent to the number of protruding objects passing through the defined boundary. Our classification builds upon this observation, having the following domain assumptions in mind:

- 0 clusters in the bounding manifold indicate a lack of connected adjacent structure, hence, the segmented structure corresponding to a solitary nodule,
- 1 cluster in the bounding manifold indicates a single connection to an attached structure, which in many cases originates from a nodule attached to larger structures, like the lung wall, etc.
- 2 clusters indicates two connections, which is most often observed for blood vessels, and
- >3 clusters indicate a vessel junction.

We propose to identify the *number of high intensity clusters* through a clustering algorithm. The clustering strategy chosen is based on the widely used principle of EM-based fitting of Gaussians. In addition to those of the standard EM Gaussian clustering, our variant requires to obey the following important properties:

1. Our bounding manifold representation is parameterized by the spherical angular variables $\theta$ and $\phi$, which correspond to so-called *directional data*.[12] Hence, our clustering needs to reflect in particular the continuities in the $(\theta, \phi)$-domain that appear at the edge of the 2D bounding manifold image. For an illustration of this problem, consider the simplified illustration of Figure 3 and the caption thereof.
2. The number of modes has to be determined automatically.

**Directional data modeling** For statistical modeling of directional data, there are a number of models that have been proposed previously. One is the *von Mises-Fisher distribution*.[12] In fact, EM-based clustering of von Mises-Fisher distributions has been proposed very recently.[13] However, parameter estimation for the von Mises-Fisher distribution involves solving an implicit equation of a ratio of Bessel functions, for which no analytic solution exists, in general.

For this study, we utilize an alternative modeling, which allows a less restrictive parameter estimation than the von Mises-Fisher modeling. It is the *multivariate wrapped Gaussian distribution*,[11] which is an extension of the wrapped Gaussian distribution.[12]

We briefly introduce the concept. For further details it is referred to literature.[11, 12] A Gaussian distribution $\mathcal{N}(x)$ of a variable $x$ on the line can be "wrapped" around the circumference of a circle of unit radius. That is, the wrapped Gaussian distribution $\mathcal{N}_{\mathrm{w}}(\vartheta)$ of the wrapped variable

$$\vartheta = x_{\mathrm{w}} = x \bmod 2\pi \quad \in (-\pi, \pi]$$

is

$$\mathcal{N}_{\mathrm{w}}(\vartheta) = \sum_{k=-\infty}^{\infty} \mathcal{N}(\vartheta + 2\pi k).$$

A multivariate wrapped Gaussian distribution of a vector variable $\boldsymbol{\vartheta} = (\vartheta_1, \ldots, \vartheta_F)^T$ can be defined similarly as

$$\mathcal{N}_{\mathrm{w}}(\boldsymbol{\vartheta}) = \sum_{k_1=-\infty}^{\infty} \cdots \sum_{k_F=-\infty}^{\infty} \mathcal{N}(\boldsymbol{\vartheta} + 2\pi k_1 \mathbf{e}_1 + \cdots + 2\pi k_F \mathbf{e}_F), \tag{1}$$

where $\mathbf{e}_k = (0, \ldots, 0, 1, 0, \ldots, 0)^T$ is the $k$-th Euclidean basis vector (with an entry of 1 at the $k$-th element and 0 elsewhere). Figure 3 shows an example of a two dimensional multivariate wrapped Gaussian.

It has been shown[11] that, given an appropriately small variance in the directional variables, accurate mean and covariance estimates $\hat{\mu}_{\boldsymbol{\vartheta}}$ and $\hat{\boldsymbol{\Sigma}}_{\boldsymbol{\vartheta}}$ for Equation 1 can be obtained from a sample set $\mathbb{X} = \left\{\boldsymbol{\vartheta}^{(1)}, \ldots, \boldsymbol{\vartheta}^{(M)}\right\}$ using

$$(\hat{\mu}_{\boldsymbol{\vartheta}})_f = \arg\left(\frac{1}{M}\sum_{m=1}^{M} e^{J\vartheta_f^{(m)}}\right) \tag{2}$$

and

$$\hat{\boldsymbol{\Sigma}}_{\boldsymbol{\vartheta}} = \frac{1}{M-1}\sum_{m=1}^{M} \boldsymbol{\vartheta}^{(m)\prime}\boldsymbol{\vartheta}^{(m)\prime T} \tag{3}$$

with

$$\vartheta^{(m)\prime} = \left(\vartheta_f^{(m)} - (\hat{\mu}_{\boldsymbol{\vartheta}})_f\right) \bmod 2\pi,$$

$J^2 = -1$ the imaginary unit, and "arg" the phase of a complex number. For simplicity, a periodicity of $2\pi$ and range of $\vartheta_f \in (-\pi, \pi]$ has implicitly been assumed for all dimensions $f$ in $\boldsymbol{\vartheta}$.

In the context of the EM clustering algorithm, we can simply replace the regular, linear Gaussian model with the above sketched multivariate wrapped Gaussian model. In particular, Equation (1) on the one hand and Equations (2) and (3) on the other hand replace the original linear equivalents in the E and the M step, respectively. Readers can verify a result of the multivariate wrapped Gaussian EM clustering in Figures 4, row 3 and 4 as well as Figure 5, row 3 and 4.

**EM clustering with integrated model selection** In the context of EM-based clustering, several extensions have been proposed for automatic mode number selection in the past. We base our solution on a recent publication,[10] which integrates finite mixture of Gaussian estimation and model selection, using minimum description length (MDL) criterion, into a single algorithm.

Note that, in general, input to EM clustering algorithms is a sample set $\mathbb{X} = \{(\theta_1, \phi_1), \ldots, (\theta_M, \phi_M)\}$ of observations, whereas the present data is the 2D (image) matrix $I(\theta, \phi)$. To overcome this incompatibility, we draw observations $\mathbb{X}$ directly from $I(\theta, \phi)$, where the number of occurrences of each sampled $(\theta_m, \phi_m) \in (-\pi, \pi] \times (-\pi, \pi]$ is set proportional to the corresponding image matrix value $I(\theta_m, \phi_m)$.

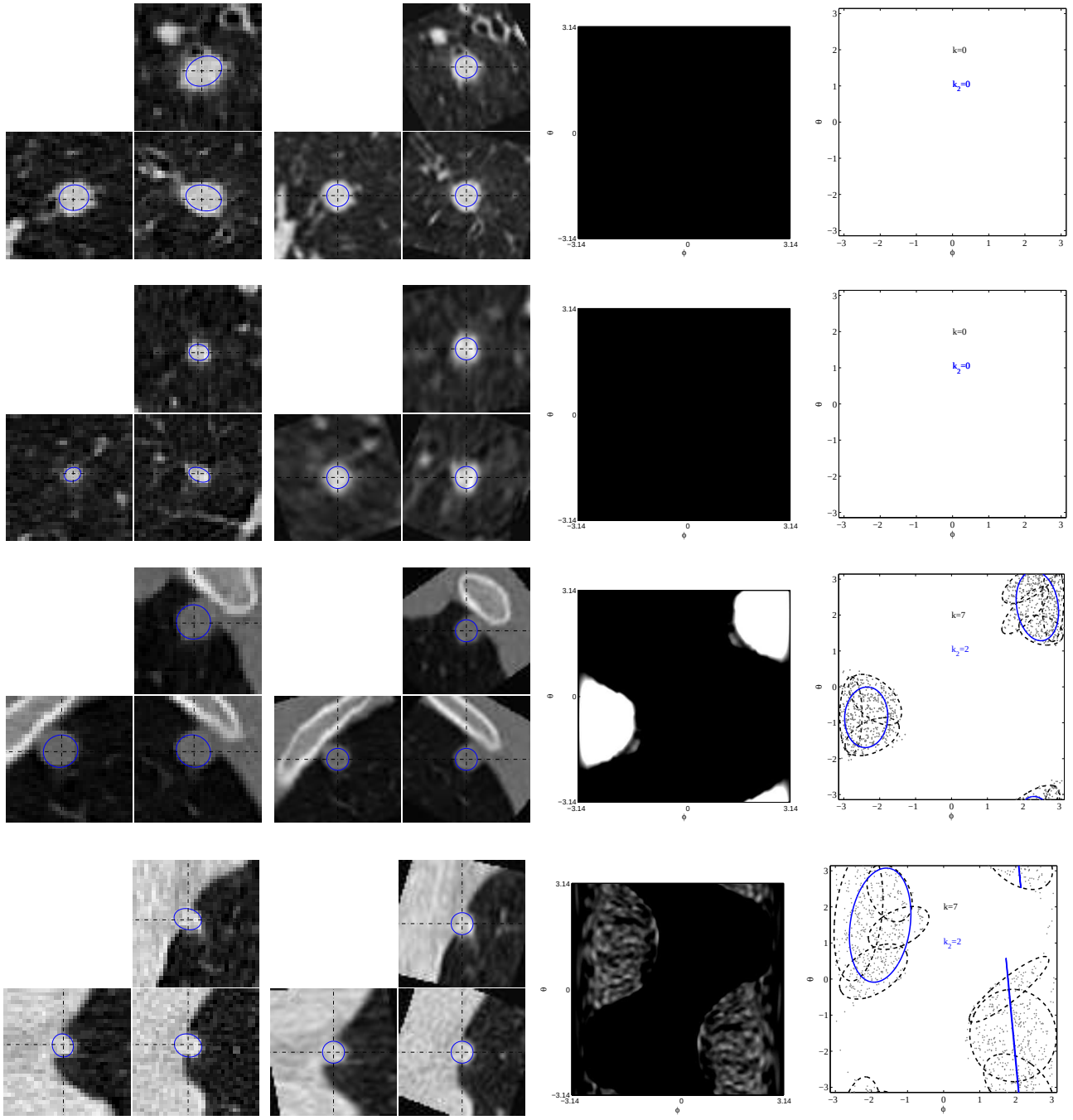


(a) VOI and segmented nodule candidate

(b) Affine-normalized VOI

(c) Thresholded unwrapped bounding manifold

(d) Result of clustering and cluster postprocessing

**Figure 4.** This figure shows illustrative examples of the proposed pulmonary structure classification method for thoracic CT scans. Each row corresponds to the segmentation and verification of one example, the first two rows with respect to a nodule object, the last two rows with respect to nodules attached to the lung wall. (Cf. Figure 5 for similar illustrations with vessel and vessel junction examples.) Column (a) illustrates the CT VOI in three orthogonal cross sections. The result of our segmentation is illustrated by the ellipses. Column (b) represents the affine-normalization of the original VOI, such that the 3D ellipsoid becomes warps to a sphere. Column (c) shows the constructed bounding manifold, including an additional intensity thresholding, unwrapped in the $(\theta, \phi)$-domain. The figures in column (d) show the results of the Gaussian mixture model fitting by the EM-based algorithm. Dashed ellipses correspond to EM-based clustered Gaussian components, the solid ellipses describe the clusters after post-processing.

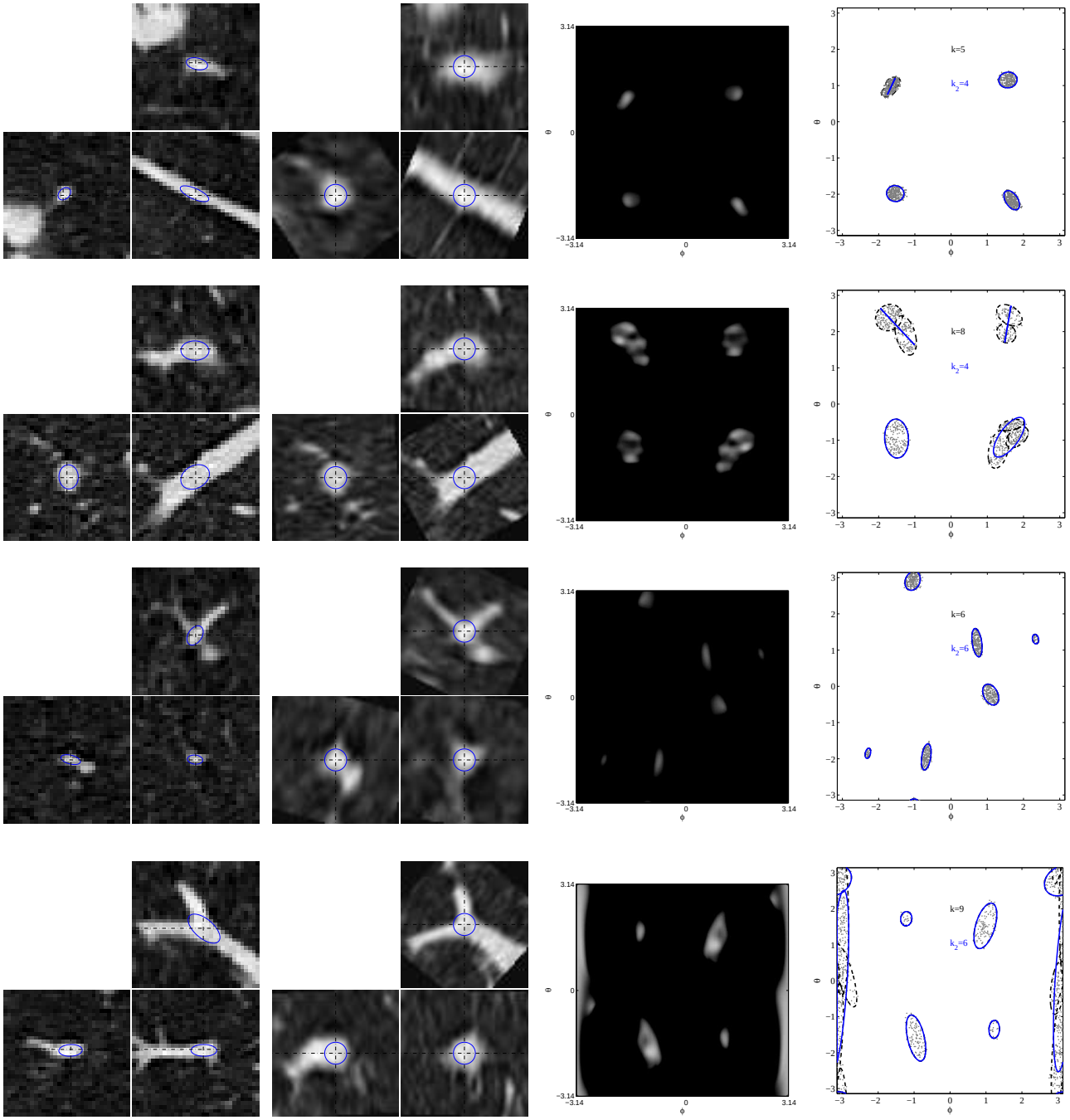


(a) VOI and segmented nodule candidate

(b) Affine-normalized VOI

(c) Thresholded unwrapped bounding manifold

(d) Result of clustering and cluster postprocessing

**Figure 5.** This figure is an extension of Figure 4. For explanation, please refer to the caption thereof. Row 1 and 2 show vascular structures, row 3 and 4 vessel junctions.

**Cluster post-processing** One problem with the Gaussian EM clustering can arise if one of the true protruding structure shapes in the bounding manifold do not correspond to the elliptical Gaussian shape. In such cases, it is expected that the EM algorithm fits this structure with a set of Gaussian components. Such an effect would clearly affect our classification adversely, where the *number* of components plays an integral role. To deal with this problem, we propose to apply a post-processing, which aims to merge appropriate components.

In particular, this post-processing can be seen as a second cluster analysis, which analyzes the set of all EM-fitted Gaussian components and merges subsets to a single cluster — up to a certain scale. A very flexible and widely used technique for such problems is agglomerative hierarchical clustering.[14] In hierarchical clustering, the cluster space is expressed in terms of distances of its elements. In the present case elements are multivariate wrapped Gaussian functions. In conformity with previous proceeding in this paper, we make use of statistical descriptors for the geometric shapes. A suitable (and analytically computable) statistical distance measure for Gaussian distributions is the Bhattacharyya distance

$$D_{\text{Bhatt}}\left(\boldsymbol{\mu}_1, \boldsymbol{\Sigma}_1, \boldsymbol{\mu}_2, \boldsymbol{\Sigma}_2\right) = \frac{1}{8}\left(\boldsymbol{\mu}_2 - \boldsymbol{\mu}_1\right)^T \left(\frac{\boldsymbol{\Sigma}_1 + \boldsymbol{\Sigma}_2}{2}\right)^{-1} \left(\boldsymbol{\mu}_2 - \boldsymbol{\mu}_1\right) + \frac{1}{2}\ln\frac{\left|\boldsymbol{\Sigma}_1 + \boldsymbol{\Sigma}_2\right|}{\sqrt{\left|\boldsymbol{\Sigma}_1\right|\left|\boldsymbol{\Sigma}_2\right|}}.$$

However, $D_{\text{Bhatt}}$ does not take into account the directional characteristics of the wrapped Gaussians. Hence we propose a slightly modified variant of $D_{\text{Bhatt}}$, the "wrapped Bhattacharyya distance"

$$D^{\text{w}}_{\text{Bhatt}}\left(\boldsymbol{\mu}_1, \boldsymbol{\Sigma}_1, \boldsymbol{\mu}_2, \boldsymbol{\Sigma}_2\right) = \frac{1}{8}\left(\left(\boldsymbol{\mu}_2 - \boldsymbol{\mu}_1\right) \bmod 2\pi\right)^T \left(\frac{\boldsymbol{\Sigma}_1 + \boldsymbol{\Sigma}_2}{2}\right)^{-1} \left(\left(\boldsymbol{\mu}_2 - \boldsymbol{\mu}_1\right) \bmod 2\pi\right) + \frac{1}{2}\ln\frac{\left|\boldsymbol{\Sigma}_1 + \boldsymbol{\Sigma}_2\right|}{\sqrt{\left|\boldsymbol{\Sigma}_1\right|\left|\boldsymbol{\Sigma}_2\right|}}.$$

Finally, the number of wrapped Gaussian component clusters, in the experiments referred to as $k_2$, determines the class of the pulmonary structure: 0 for a solitary nodule, $2 \cdot 1 = 2$ for an attached nodule, $2 \cdot 2 = 4$ for a vessel, and $> 2 \cdot 3 = 6$ for vessel junction. The factor of 2 is due to the double interval in the polar coordinate $\phi$, as discussed in Section 2.2.1.

## 3. EXPERIMENTS

In this contribution, we present qualitative experiments for the proposed pulmonary structure classification. Figures 4 and 5 show illustrations of the classification for thoracic CT images, two examples for each of the classes "nodule", "attached nodule", "vessel", "vessel junction".

As presented in column (a), the 3D segmentation method (as sketched in Section 2.1) can segment all solitary and attached nodules (Figure 4) as well as the false positive blood vessels and vessel junctions (Figure 5). Column (b) illustrates the respective VOIs after affine-normalization. Column (c) shows the bounding manifold, which is constructed from the procedure described in Section 2.2.1. Note, however, that an additional intensity thresholding has been introduced. This step is applied as a fast and simple means for eliminating low-intensity structures, which may confuse the Gaussian EM clustering. In column (d) the bounding manifold image is transformed to a sampled data set $\mathbb{X}$, as it has been described in Section 2.2.1. Further, column (d) shows the result of the EM-based wrapped Gaussian clustering, that is, mean and covariance of the $k$ components are illustrated by the dashed ellipses. In particular, note the continuities at the edges of the $(\theta, \phi)$-domain in Figures 4, row 3 and 4, and Figure 5, row 3 and 4. For visualization purposes, we have also included an illustration of the hierarchical clustering post-processing. Clusters from this post-processing are represented by the $k_2$ solid ellipses, the center point and spread of which correspond to mean and covariance computed from means of all wrapped Gaussians within one post-processed cluster. Note that this illustration may lead to degenerated ellipses, for instance in Figure 5, row 2, if the cluster cardinality is low. Inferring the structure class from the component number $k_2$, it can be verified that the presented classification gives correct answer for all eight examples. Similar results were obtained with other cases.

It is worthwhile to point out limitations of the algorithm, which may lead to misclassifications in some situations. Structures at the poles of the manifold 3D sphere (corresponding to $\phi = 0$ and $\phi = \pi$) become disproportionately large in the $\theta$-dimension of the 2D image after the unwrapping. This situation can be compared with a phenomenon from cartography where arctic and antarctic regions occupy comparably larger regions on a 2D world map than on the 3D spherical world globe. In the examples illustrated above, this behavior can be observed in Figure 5, row 4, where the high intensity structure at $\phi \approx \pi$ extends over the entire range $(-\pi, \pi]$ in $\theta$. As a consequence, caution is advised, when drawing conclusions from scale relations in the unwrapped manifold, in particular, for those pole regions. This is, in fact, a drawback of the wrapped Gaussian modeling, in particular, the unwrapping. At this point, it shall be noted that the above mentioned von Mises-Fisher modeling circumvents this phenomenon, because no unwrapping is assumed.

## 4. CONCLUSION

We have proposed a novel method of classifying pulmonary structures, such as nodules, attached nodules, vessels and vessel junctions. Such a classification can be advantageously applied in a CAD system for nodule detection, in particular, for false positive removal. Further, VOI representations chosen in the parts of the modeling have beneficial visualization capabilities, in particular the unwrapped 2D bounding manifold of Figure 1 (c). This is an important advantage in the context of a user (radiologist) interaction.

Main elements of the presented classification include (i) a module for anisotropic Gaussian fitting, (ii) a construction of a 2D manifold at the boundary of the pulmonary structure, and (iii) a robust cluster analysis of this manifold. Part (i) is based on our previous work. For part (ii), we have proposed a data driven scale selection based on entropy minimization. For the solution of part (iii), we have brought together powerful statistical analysis methods, such as EM-based clustering with automatic mode number selection, directional data modeling, and hierarchical clustering based on a variant of the Bhattacharyya distance. Unlike other global methods such as vessel tree reconstruction, this method allows for the localized flexible examination of pulmonary structures.

We have shown a qualitative study with thoracic CT images and demonstrated and illustrated favorable classification results in this domain. The presented algorithm could robustly classify examples of nodules, attached nodules, vessels and vessel junctions.

Building on these promising results, we plan to perform quantitative performance validation in order to show the effectiveness of the proposed solution in more clinically relevant settings. A main limitation of the proposed method is the fact that scales are position dependent within the $(\theta, \phi)$-domain. In this respect, future research should focus on improving this deficiency. For instance, modeling with von Mises-Fisher distribution could circumvent this problem. Complementary to the statistical clustering approach, we want to pursue the idea of mode number detection based on connected component approaches. Similar to the proposed wrapped Gaussian modeling, such an approach needs to address the directional characteristics in spheres. Another possible improvement concerns the use of more topological knowledge. So far, classification is solely based on the *number* of identified protruding structures. Certainly, additional information lies in their size and relative position. For further studies, we plan to incorporate this extra information.

## 5. ACKNOWLEDGMENTS

The authors like to thank Imad Zoghlami and Visvanathan Ramesh from Siemens Corporate Research for very helpful discussions.

## REFERENCES

1. H. K. Weir et al., "Annual report to the nation on the status of cancer, 1975-2000," *Journal of the National Cancer Institute* **95**(17), pp. 1276–1299, 2003.
2. F. Li, C. Novak, J. Qian, G. Kohl, and D. Naidich, "Automatic detection of lung nodules from multi-slice low-dose ct images," in *Medical Imaging 2001: Image Processing*, pp. 1828–35, (San Diego, CA), 2001.
3. Y. Lee, T. Hara, H. Fujita, S. Itoh, and T. Ishigaki, "Automated detection of pulmonary nodules in helical CT images based on an improved template-matching technique," *IEEE Trans. Medical Imaging* **20**(7), pp. 595–604, 2001.
4. S. Chang, H. Emoto, D. N. Metaxas, and L. Axel, "Pulmonary micronodule detection from 3D chest CT," in *7th Medical Image Computing and Computer Assisted Intervention (MICCAI)*, **2**, pp. 821–828, 2004.
5. Y. Kawata, N. Niki, H. Ohmatsu, M. Kusumoto, R. Kakinuma, K. Yamada, K. Mori, H. Nishiyama, K. Eguchi, M. Kaneko, and N. Moriyama, "Pulmonary nodule classification based on nodule retrieval from 3-d thoracic CT image database," in *7th Medical Image Computing and Computer Assisted Intervention (MICCAI)*, **2**, pp. 838–846, 2004.
6. A. A. Farag, A. El-Baz, G. L. Gimel'farb, R. Falk, and S. G. Hushek, "Automatic detection and recognition of lung abnormalities in helical ct images using deformable templates," in *7th Medical Image Computing and Computer Assisted Intervention (MICCAI)*, **2**, pp. 856–864, 2004.
7. G. Agam, S. G. Armato III, and C. Wu, "Vessel tree reconstruction in thoracic CT scans with application to nodule detection," *IEEE Trans. Medical Imaging* **24**(4), 2005.

8. Y. Fridman, S. M. Pizer, S. R. Aylward, and E. Bullitt, “Segmenting 3D branching tubular structures using cores,” in *6th Medical Image Computing and Computer Assisted Intervention (MICCAI)*, **2**, 2003.
9. K. Okada, D. Comaniciu, and A. Krishnan, “Robust anisotropic Gaussian fitting for volumetric characterization of pulmonary nodules in multislice CT,” *IEEE Trans. Medical Imaging* **24**(3), pp. 409–423, 2005.
10. M. Figueiredo and A. Jain, “Unsupervised learning of finite mixture models,” *IEEE Trans. Pattern Anal. and Mach. Intell.* **24**(3), pp. 381–396, 2002.
11. C. Bahlmann, “Directional features in online handwriting recognition,” *Pattern Recognition* **39**, Jan. 2006.
12. K. V. Mardia, *Statistics of Directional Data*, Academic Press, 1972.
13. A. Banerjee, I. S. Dhillon, J. Ghosh, and S. Sra, “Clustering on the unit hypersphere using von Mises-Fisher distributions,” *Journal of Machine Learning Research* (9), pp. 1345–1382, 2005.
14. S. Theodoridis and K. Koutroumbas, *Pattern Recognition*, Academic Press, 1999.